Stepwise Charge Separation in Heterotriads. Binuclear Ru(II)−Rh(III) Complexes on Nanocrystalline Titanium Dioxide

Cornelis J. Kleverlaan,[†] M. Teresa Indelli,[†] Carlo A. Bignozzi,[†] Luiz Pavanin,[†,‡] Franco Scandola,*[,†] Georg M. Hasselman,[§] and Gerald J. Meyer[§]

Contribution from the Dipartimento di Chimica, Università di Ferrara, 44100 Ferrara, Italy, and the Department of Chemistry, Johns Hopkins University, Baltimore, Maryland

Received August 2, 1999. Revised Manuscript Received December 7, 1999

Abstract: Two novel Ru(II)-Rh(III) polypyridine dyads, containing carboxylic functions at the Rh(III) unit, $Rh^{III}(dcb)_2$-(BL)-$Ru^{II}(dmp)_2$ and $Rh^{III}(dcb)_2$-(BL)-$Ru^{II}(bpy)_2$ (bpy = 2,2′-bipyridine; dcb = 4,4′-dicarboxy-2,2′-bipyridine; dmp = 4,7-dimethyl-1,10-phenanthroline; BL = 1,2-bis[4-(4′-methyl-2,2′-bipyridyl)]ethane), have been synthesized. Their photophysical behavior in solution, compared with that of the mononuclear $Ru^{II}(dcb)_2(dmb)$ model (dmb = 4,4′-dimethyl-2,2′-bipyridine), indicates the occurrence of fast (10^8-10^9 s^{-1}) and efficient (>95%) Rh(III)-*Ru(II) → Rh(II)-Ru(III) photoinduced electron transfer. These species adsorb firmly on nanoporous TiO_2 films, via the dcb ligands of the Rh(III) units. The behavior of the adsorbed species has been studied by means of nanosecond time-resolved emission and absorption measurements, as well as by photocurrent measurements. Photocurrent action spectra demonstrate that light absorption by the Ru(II) chromophore leads to electron injection into the semiconductor. A detailed analysis of the transient behavior of the TiO_2-$Rh^{III}(dcb)_2$-(BL)-$Ru^{II}(bpy)_2$ system indicates that about one-third of the adsorbed dyads (probably because of different orientation at the surface or accidental contacts in small cavities) undergo direct electron injection from the excited state of the Ru(II) chromophore. The remaining dyads display stepwise charge injection processes, i.e., intramolecular electron transfer, TiO_2-Rh(III)-*Ru(II) → TiO_2-Rh(II)-Ru(III), followed by charge separation by electron injection,TiO_2-Rh(II)-Ru(III) → $TiO_2(e^-)$-Rh(III)-Ru(III). The first process has comparable rates and efficiencies as for the free dyads in solution. The second step is 40% efficient, because of competing primary recombination, TiO_2-Rh(II)-Ru(III) → TiO_2-Rh(III)-Ru(II). When the final recombination between injected electrons and oxidized Ru(III) centers is studied, a remarkable slowing down is obtained for the supramolecular systems, e.g., TiO_2-$Rh^{III}(dcb)_2$-(BL)-$Ru^{II}(bpy)_2$, relative to analogous systems containing simple mononuclear sensitizers, e.g., TiO_2-$Ru^{II}(dcb)_2(dmb)$. Stepwise charge separation and slow recombination between remote sites are distinctive features that suggest the labeling of these systems as "heterotriads".

Introduction

Central to supramolecular chemistry[1−5] is the concept that, at difference with simple molecular systems, suitable assemblies of molecular components (supramolecular structures) can be designed to perform relatively elaborate and useful tasks (*functions*). This idea has received great impulse from recent progress in the understanding of the structure−function relationship in many natural systems, photosynthetic membranes[6−14] being a prominent example. The concept is currently being applied to the design of supramolecular systems ("molecular devices") capable of mimicking, at the molecular level, functions normally performed by a natural system or by artificial macroscopic devices. Examples are light-harvesting antenna systems,[15−18] artificial reaction centers,[19−23] molecular switches,[24]

[†] Università di Ferrara.

[‡] Permanent address: Departamento de Quimica, Universidade de Uberlandia, Uberlandia, Brasil.

[§] Johns Hopkins University.

(1) Lehn, J.-M. *Angew. Chem., Int. Ed. Engl.* **1988**, *27*, 89. Lehn, J.-M. *Angew. Chem., Int. Ed. Engl.* **1990**, *29*, 1304.

(2) Lehn, J.-M. *Supramolecular Chemistry*; VCH: Weinheim, Germany, 1995.

(3) *Comprehensive Supramolecular Chemistry*; Atwood, J. L., Davies, J. E. D., MacNicol, D. D., Vögtle, F., Eds.; Pergamon/Elsevier: Oxford, 1996.

(4) Balzani, V.; Scandola, F. *Supramolecular Photochemistry*; Horwood: Chichester, 1991.

(5) Balzani, V.; Scandola, F. In *Comprehensive Supramolecular Chemistry*; Reinhoudt, D. N., Ed.; Pergamon Press: Oxford, 1996; Vol. 10, p 687.

(6) Deisenhofer, J.; Epp O.; Miki, K.; Huber, R.; Michel, H. *J. Mol. Biol.* **1984**, *180*, 385.

(7) Chang, C.-H.; Tiede, D. M.; Tang, J.; Smith, U.; Norris, J.; Schiffer, M. *FEBS Lett.* **1986**, *205*, 82.

(8) Allen, J. P.; Feher, G.; Yeates, T. O.; Komiya, H.; Rees, D. C. *Proc. Natl. Acad. Sci. U.S.A.* **1987**, *84*, 5730.

(9) Deisenhofer, J.; Michel, H. *Angew. Chem., Int. Ed. Engl.* **1989**, *28*, 829.

(10) Huber, R. *Angew. Chem., Int. Ed. Engl.* **1989**, *28*, 848.

(11) McDermott, G.; Prince, S. M.; Freer, A. A.; Hawthornthwaite-Lawless, A. M.; Papiz, M. Z.; Cogdell, R. J.; Isaacs, N. W. *Nature* **1995**, *374*, 517.

(12) Kuhlbrandt, W. *Nature* **1995**, *374*, 497.

(13) Karrasch, S.; Bullough, P. A.; Ghosh, R. *EMBO J.* **1995**, *14*, 631.

(14) Kuhlbrandt, W.; Wang, D. N.; Fujiyoshi, Y. *Nature* **1994**, *367*, 1994.

(15) Amadelli, R.; Argazzi, R.; Bignozzi, C. A.; Scandola, F. *J. Am. Chem. Soc.* **1990**, *112*, 7099.

(16) Balzani, V.; Campagna, S.; Denti, G.; Juris, A.; Serroni, S.; Venturi, M. *Acc. Chem. Res.* **1998**, *31*, 26.

(17) (a) Prathapan, S.; Johnson, T. E.; Lindsey, J. S. *J. Am. Chem. Soc.* **1993**, *115*, 7519. (b) Hsiao, J.-S.; Krueger, B. P.; Wagner, R. W.; Johnson, T. E.; Delaney, J. K.; Mauzerall, D. C.; Fleming, G. R.; Lindsey, J. S.; Bocian, D. F.; Donohoe, R. J. *J. Am. Chem. Soc.* **1996**, *118*, 11181.

(18) Bignozzi, C. A.; Schoonover, J. R.; Scandola, F. *Prog. Inorg. Chem.* **1997**, *44*, 1.

(19) Wasielewski, M. R. *Chem. Rev.* **1992**, *92*, 435.

10.1021/ja992755f CCC: $19.00
Published on Web 03/14/2000

logic gates,[25,26] shift registers,[27] optoelectronic gates,[28] fluorescent sensors,[29−32] molecular machines,[33−35] etc. In many of these artificial molecular devices, a fundamental role is played by light (either as an energy input or as a signal to be processed), and the function relies on energy or electron-transfer processes taking place, with controlled rates and in appropriate sequences, between molecular components of the supramolecular structure. From this standpoint, supramolecular chemistry (and photochemistry) can be viewed as the basis for a "*bottom-up*" approach[36] to the challenging fields of molecular electronics[37−39] and nanotechnology.[40−42]

Interestingly, the opposite, "*top-down*" tendency is active in the field of materials science, where increasing attention is being shifted from bulk materials to systems of smaller and smaller dimensions (colloids, nanoparticles, nanocrystalline materials). For various semiconductors, particles of controlled nanometer size now can be prepared,[43] functionalized,[44] and assembled in various types of ordered arrays, mesoscopic architectures, etc.[45] It can be noticed that, working in opposite directions, these two types of approach converge to objects of the same, nanometer size. Thus, an appealing idea is that of coupling together, via covalent bonding or other interactions, supramolecular systems and nanoparticles in what can be called "heterosupramolecular"[46] systems. In such systems, individual nanoparticles can be photoexcited, participate in excitation energy transfer processes, behave as electron acceptors or electron donors, etc., i.e., play the role of additional molecular components of the supramolecular assembly. Nanoparticles, however, also possess solid-state properties and, as part of macroscopic aggregates (superlattices, nanoporous substrates), can provide an interface between the supramolecular system and the external word. This brings along interesting prospectives for addressing, modulating, or exploiting the supramolecular function.

Molecular species chemically linked to the surface of nanocrystalline materials have been actively investigated in recent years, particularly to exploit the principles of spectral sensitization of wide-band gap semiconductors[47] for light energy conversion purposes. The classical example, from the efficient solar cell developed by Grätzel and co-workers,[48] is *cis*-$Ru(dcb)_2(NCS)_2$ on TiO_2. In homogeneous solution, covalently linked chromophore−acceptor systems used for the study of photoinduced charge separation and recombination are commonly called dyads.[5] By analogy, the sensitizer−nanoparticle assembly can be viewed as a "heterodyad". In the homogeneous field, there has been a trend toward improving the performance by increasing the complexity of the supramolecular systems (e.g., going from dyads to triads, etc.).[5,16,17,20−22] We have recently pointed out some potential advantages of an evolution of the heterogeneous systems in the same direction.[18] In particular, incorporating multichromophoric structures into the sensitizer unit can increase the light-harvesting efficiency, and going from mononuclear sensitizers to polynuclear sensitizers could be used as a means to increase the distance and lifetime of charge separation. Of the two possible heterotriad schemes shown in Figure 1, that of Figure 1b has been recently implemented.[49,50] We wish to present here a proof-of-principle case for the scheme of Figure 1a. The starting point is our previous experience with Ru(II)-Rh(III) ligand-bridged polypyridine complexes,[51−53] where photoexcitation of the Ru(II) unit triggers fast electron transfer to the Rh(III) unit. The idea was to obtain TiO_2-Rh(III)-Ru(II) heterotriads, by selective grafting of such type of dyads on nanocrystalline titanium dioxide. To this aim, two appropriately functionalized Ru(II)-Rh(III) dyads have been designed and synthesized. The dyads, schematized in Figure 2 in their fully protonated form, are abbreviated[54] as $Rh^{III}(dcb)_2$-(BL)-$Ru^{II}(dmp)_2$ and $Rh^{III}(dcb)_2$-

(20) Gust, D.; Moore, T. A.; Moore, A. L. *Acc. Chem. Res.* **1993**, *26*, 198.
(21) Liddell, P. A.; Kuciauskas, D.; Sumida, J. P.; Nash, B.; Nguyen, D.; Moore, A. L.; Moore, T. A.; Gust, D. *J. Am. Chem. Soc.* **1997**, *119*, 1400−1405.
(22) Harriman, A.; Sauvage, J. P. *Chem. Soc. Rev.* **1996**, 41.
(23) Slate, C. A.; Striplin, D. R.; Moss, J. A.; Chen, P.; Erickson, B. W.; Meyer, T. J. *J. Am. Chem. Soc.* **1998**, *120*, 4885
(24) Gilat, S. L.; Kawai, S. H.; Lehn, J.-M. *J. Chem. Soc., Chem. Commun.* **1993**, 1439.
(25) de Silva, A. P.; Gunaratne, H. Q. N.; McCoy, C. P. *Nature* **1993**, *364*, 42.
(26) Credi, A.; Balzani, V.; Langford, S. J.; Stoddart, J. F. *J. Am. Chem. Soc.* **1997**, *119*, 2679.
(27) Hopfield, J. J.; Onuchic, J. N.; Beratan, D. N. *Science* **1988**, *241*, 817.
(28) Wagner, R. W.; Lindsey, J. S.; Jyoti, S.; Palaniappan, V.; Bocian, D. F. *J. Am. Chem. Soc.* **1966**, *118*, 3996.
(29) de Silva, A. P.; Gunaratne, H. Q. N.; Gunnlaugsson, T.; Huxley, A. J. M.; McCoy, C. P.; Rademacher, J. T.; Rice, T. E. *Chem. Rev.* **1997**, *97*, 1515.
(30) Masilamani, D.; Lucas, M. E. *ACS Symp. Ser.* **1993**, *538*, 162.
(31) Czarnik, A. W. *Acc. Chem. Res.* **1994**, *27*, 302.
(32) James, T. D.; Sandanayake, K. R. A. S.; Shinkai, S. *Angew. Chem., Int. Ed. Engl.* **1994**, *33*, 2207.
(33) Ashton, R. R.; Ballardini, R.; Balzani, V.; Constable, E. C.; Credi, A.; Kocian, O.; Langford, S. J.; Preece, J. A.; Prodi, L.; Schofield, E. R.; Spencer, N.; Stoddard, J. F.; Wenger, S. *Chem. Eur. J.* **1988**, *4*, 2413.
(34) Balzani, V.; Gomez-Lopez, M.; Stoddart, J. F. *Acc. Chem. Res.* **1998**, *31*, 405.
(35) Sauvage, J.-P. *Acc. Chem. Res.* **1998**, *31*, 611.
(36) Feynman, R. P. *Sat. Rev.* **1960**, *43*, 45.
(37) *Molecular Electronic Devices*; Carter, F. L., Siatkowsky, R. E., Woltjien, H., Eds.; Elsevier: Amsterdam, 1988.
(38) *Molecular Electronics*; Jortner, J., Ratner, M., Eds.; Blackwell: London, 1997.
(39) Rouvray, D. *Chem. Br.* **1998**, *34*, 26.
(40) Drexler, K. E. *Nanosystems: Molecular Machinery, Manufacturing, and Computation*; Wiley: New York, 1992.
(41) *Nanostructures based on Molecular Materials*; Göpel, V., Ziegler, C., Eds.; VCH: Weinheim, 1992.
(42) Bard, A. J. *Integrated Chemical Systems*; Wiley: New York, 1994.
(43) (a) Henglein, A. *Chem. Rev.* **1989**, *89*, 1861. (b) Murray, C. B.; Norris, D. J.; Bawendi *J. Am. Chem. Soc.* **1993**, *115*, 8706. (c) Kotov, N.; Meldrum, F.; Fendler, J. *J. Phys. Chem.* **1994**, *98*, 8827.
(44) (a) Marguerettaz, X.; O'Neill, R.; Fitzmaurice, D. *J. Am. Chem. Soc.* **1994**, *116*, 2629. (b) Kamat, P. V. *Prog. Inorg. Chem.* **1997**, *44*, 273.
(45) (a) Murray, C. B.; Kagan, C. R.; Bawendi, M. G. *Science* **1995**, *270*, 1335. (b) Peng, X.; Wilson, T.; Alivisatos, P.; Schultz, P. *Angew. Chem., Int. Ed. Engl.* **1997**, *36*, 145. (c) Cusack, L.; Rizza, R.; Gorelov, A.; Fitzmaurice, D. *Angew. Chem., Int. Ed. Engl.* **1997**, *36*, 848. (d) Rizza, R.; Fitzamaurice, D.; Hearne, S.; Hugues, G.; Spoto, G.; Ciliberto, E.; Kerp, H.; Schropp, R. *Chem. Mater.* **1997**, *9*, 2969.
(46) Marguerettaz, X.; Fitzmaurice, D. *J. Am. Chem. Soc.* **1994**, *116*, 5017.
(47) (a) Gerisher, H.; Willig, F. *Top. Curr. Chem.* **1976**, *61*, 33. (b) Memming, R. *Prog. Surf. Sci.* **1984**, *17*, 7. (c) Nizik, A, J.; Memming, R. *J. Phys. Chem.* **1996**, *100*, 13061.
(48) Nazeeruddin, M. K.; Kay, A.; Rodicio, I.; Humphrey-Baker, R.; Müller, E.; Loska, P.; Vlachopoulos, N.; Grätzel, M. *J. Am Chem. Soc.* **1993**, *115*, 6382.
(49) (a) Argazzi, R.; Bignozzi, C. A.; Heimer, T. A.; Castellano, F. N.; Meyer, G. J. *J. Am. Chem. Soc.* **1995**, *117*, 11815. (b) Argazzi, R.; Bignozzi, C. A.; Heimer, T. A.; Castellano, F. N.; Meyer, G. J. *J. Phys. Chem. B* **1997**, *101*, 2591.
(50) Bonhote, P.; Moser, J. E.; Vlachopoulos, N.; Walder, L.; Zakeeruddin, S. M.; Humphry-Baker, R.; Péchy, P.; Grätzel, M. *J. Chem. Soc., Chem. Commun.* **1996**, 1163. Bonhote, P.; Moser, J. E.; Vlachopoulos, N.; Walder, L.; Zakeeruddin, S. M.; Humphry-Baker, R.; Péchy, P.; Grätzel, M. *J. Am. Chem. Soc.* **1999**, *121*, 1324.
(51) Indelli, M. T.; Bignozzi, C. A.; Harriman, T.; Schoonover, J. R.; Scandola, F. *J Am. Chem. Soc.* **1994**, *116*, 3768.
(52) Indelli, M. T.; Scandola, F.; Collin, J.-P.; Sauvage, J.-P.; Sour, A. *Inorg. Chem.* **1996**, *35*, 303.
(53) Indelli, M. T.; Scandola, F.; Flamigni, L.; Collin, J.-P.; Sauvage, J.-P.; Sour, A. *Inorg. Chem.* **1997**, *36*, 4247.
(54) Abbreviations used in this paper: bpy = 2,2′-bipyridine; dmb = 4,4′-dimethyl-2,2′-bipyridine; dcb = 4,4′-dicarboxy-2,2′-bipyridine; dmp = 4,7-dimethyl-1,10-phenanthroline; BL = 1,2-bis[4-(4′-methyl-2,2′-bipyridyl)]ethane.

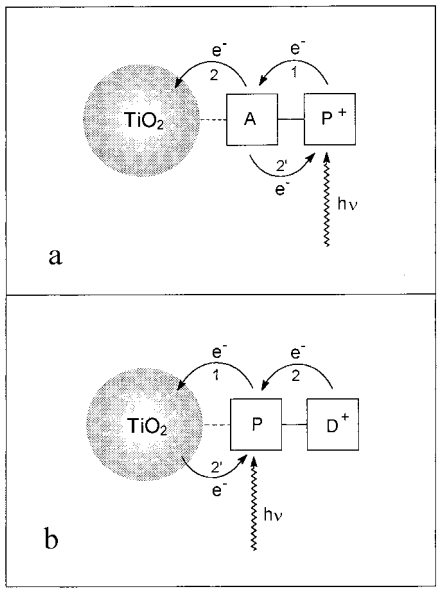

Figure 1. Schematic picture of two prototypes of heterotriads (P = photosensitizer, A = electron acceptor, D = electron donor): (a) photoinduced electron transfer from the photosensitizer P to the acceptor A, 1, is followed by injection from the reduced acceptor into the semiconductor particle, 2; (b) photoinduced electron injection from the photosensitizer P into the semiconductor particle, 1, is followed by reduction of the oxidized photosensitizer by the electron donor D, 2.

(BL)-$Ru^{II}(bpy)_2$, omitting the total charge (5+ with fully protonated carboxyl groups). The mononuclear $Ru^{II}(dcb)_2(dmb)$ complex,[54] used for comparison purposes, is also depicted in Figure 2.

Experimental Section

Materials. $(NH_4)_3RhCl_6$, $RuCl_3 \cdot 3H_2O$, 2,2′-bipyridine (bpy), 4,4′-dimethyl-2,2′-bipyridine (dmb), 4,7-dimethyl-1,10-phenathroline (dmp), and $LiOCl_4$ were purchased from Fluka. 4,4′-Dicarboxy-2,2′-bipyridine (dcb) was synthesized according to published methods.[55] The bridging ligand 1,2-bis[4-(4′-methyl-2,2′-bipyridinyl)]ethane (BL) was available from previous work.[51] The precursor complexes $Ru^{II}(bpy)_2Cl_2$ and $Ru^{II}(dmp)_2Cl_2$ were prepared according to literature methods.[56] The complex $Ru^{II}(dcb)_2(dmb)$ was prepared as described by Bignozzi and Meyer.[49] The solvents acetonitrile (MeCN) and methanol (MeOH) were of spectroscopy grade and were used as received. All the experiments were carried out at room temperature under Ar atmosphere.

Preparation of the Compounds. (a) $[Rh^{III}(dcb)_2Cl_2]Cl$. This precursor complex was prepared following a literature method,[51] with a slightly modified procedure. A 280-mg amount of $RhCl_3 \cdot 3H_2O$ (0.61 mmol) was dissolved in 5 mL of 1/1 ethanol/water and heated. To the boiling solution was added 300 mg (1.22 mmol) of dcb ligand dissolved in 20 mL of 2 M NaOH and the reaction mixture was heated to reflux for 30 min. After the mixture was cooled to room temperature, 0.25 M HCl was added dropwise until complete precipitation of a yellow solid. This product, collected by filtration, was dissolved in an aqueous NaOH diluted solution and chromatographed on G-15 Sephadex using 0.01 M NaCl as eluent. The first band contained the desired product, leaving on the column a small amount of the tris $Rh(dcb)_3^{3+}$ complex as byproduct. The first fraction was collected and concentrated to approximately 20 mL. The pH of this solution was lowered to 2.5 with HCl to obtain the complete precipitation of the protonated form of the product. The solid was washed with water and vacuum dried; 60% yield. The complex was characterized by UV−vis absorption spectrum ($(\pi-\pi^*$ bands, λ_{max} 324 nm), 77 K emission (Gaussian-shaped metal centered phosphorescence, λ_{max} 670 nm), and elemental analysis. Calcd for $[Rh(dcb)_2Cl_2]Cl \cdot 3H_2O$: C, 38.35, H, 2.95, N, 7.45. Found: C, 38.31 H, 2.31, N, 7.45.

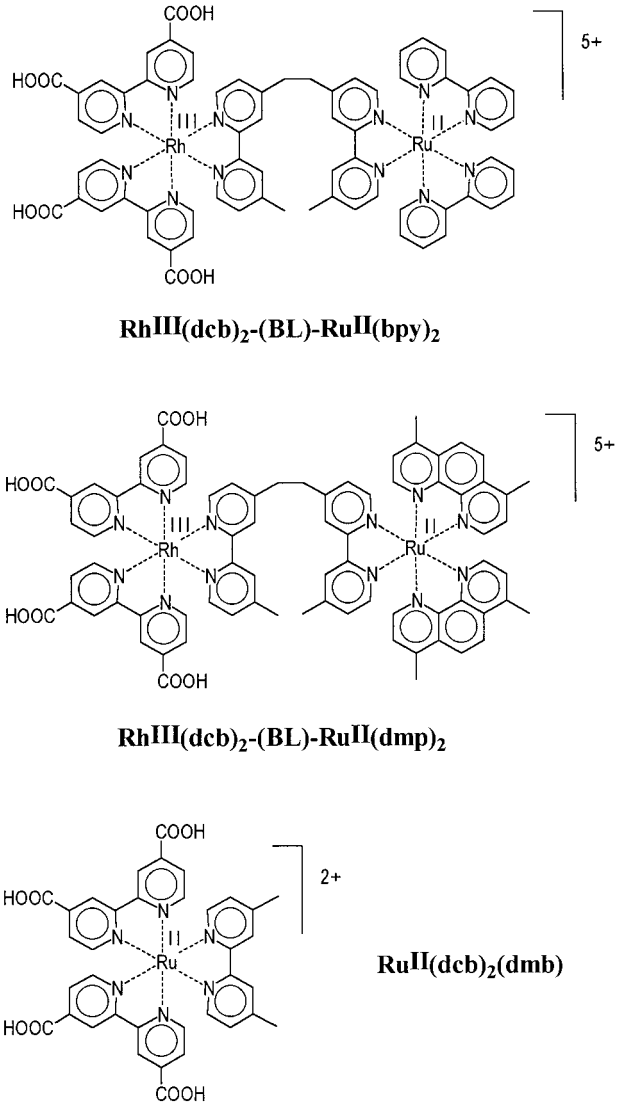

Figure 2. Schematic representation of the two dyads and the mononuclear model used.

(b) $[Rh^{III}(dcb)_2(BL)](PF_6)_3$. The synthesis of this complex was carried out starting from $[Rh^{III}(dcb)_2Cl_2]Cl$ with a 4-fold excess of BL, to minimize the formation of binuclear species. BL (630 mg,1.72 mmol) was dissolved in 50 mL of 40/60 ethylene glycol/ethanol solution and heated. To this solution was added 300 mg (0.43 mmol) of $[Rh^{III}(dcb)_2Cl_2]Cl$ separately dissolved in 25 mL of 2 M NaOH. The reaction mixture was then heated to reflux for 6 h. After evaporation of ethanol, the solution was allowed to cool to room temperature, diluted to 100 mL with water, and filtered to remove the excess BL. The pH of this filtrate was lowered to approximately 2 with a concentrated solution of HPF_6 to precipitate the product. The solid was isolated by filtration, washed well with water, and vacuum dried (70% yield). The complex was characterized by UV−vis absorption ($\pi-\pi^*$ bands, λ_{max} 316 and 304 nm), 77 K emission ($\pi-\pi^*$ structured phosphorescence, λ_{max} 455 nm), and elemental analysis. Calcd for $[Rh(dcb)_2(BL)](PF_6)_3$: C, 41.40, H, 2.75, N, 8.05. Found: C, 42.06 H, 3.1, N, 8.11. The observed differences are very likely due to small amounts of species containing incompletely protonated dcb ligands.

(c) $[Rh^{III}(dcb)_2$-(BL)-$Ru^{II}(dmp)_2](PF_6)_5$ and $[Rh^{III}(dcb)_2$-(BL)-$Ru^{II}(bpy)_2](PF_6)_5$. These dyads were prepared following the same procedure as in previous work[51] with the following modifications: reaction of the appropriate bis(polypyridine)dichloro complex of Ru(II) with $[Rh(dcb)_2(BL)](PF_6)_3$ and size exclusion chromathography on a

(55) Oki, A. R.; Morgan, R. J. *Synth. Commun*. **1995**, *25*, 4093.
(56) Sullivan, B. P.; Salomon, D. J.; Meyer, T. J. *Inorg. Chem*. **1978**, *17*, 3334.

Sephadex LH-20 resin (acetonitrile eluent) as the purification method. The complexes were identified by UV−vis and emission (see Results) and by ^{1}H NMR. The ^{1}H NMR spectra (200 MHz) were measured in CD_3CN. The chemical shifts (δ) in the aliphatic spectral region are the following: 3.2 (m, 4H), 2.64 (s, 3H), 2.52 (s, 3H) for $[Rh^{III}(dcb)_2$-(BL)-$Ru^{II}(bpy)_2](PF_6)_5$ and 3.2 (m, 4H), 2.95 (s, 6H), 2.86 (s, 6H), 2.64 (s, 3H), 2.52 (s, 3H) for $[Rh^{III}(dcb)_2$-(BL)-$Ru^{II}(dmp)_2](PF_6)_5$.

Preparation of the Films. The TiO_2 films were prepared as described by Grätzel.[48] Coating of the TiO_2 surface with the dye was carried out by soaking the film for 1−3 h in a ca. $\times 10^{-3}$ M solution of the ruthenium complex in methanol (room temperature for $Ru^{II}(dcb)_2$-(dmb) and 50 °C for $Rh^{III}(dcb)_2$-(BL)-$Ru^{II}(bpy)_2$ and $Rh^{III}(dcb)_2$-(BL)-$Ru^{II}(dmp)_2$). After completion of the dye adsorption, the film was rinsed with an excess of acetone and dried for 1 h at 60 °C. The measurements were performed directly after the preparation of the film.

Photoelectrochemistry. Photoelectrochemical measurements were performed in a two-electrode sandwich cell arrangement; a SnO_2/Pt coated glass electrode was used as the counter electrode and SnO_2/TiO_2/dye as the working electrode. The two electrodes were assembled into a "sandwich" arrangement with MeCN, 0.3 M NaI, and 0.03 M I_2 as electrolyte. The current measurements were performed with a Kontron DDM4021 Digital Multimeter. The excitation source was a 150 W Xe lamp coupled to a 0.22 m monochromator. Incident light flux was measured with a UDT-calibrated Si diode.

Apparatus. UV−vis spectra were recorded with a Kontron Uvikon 860 or HP 8453 spectrophotometer. Emission spectra were taken on a Perkin-Elmer MPF 44E spectrofluorimeter equipped with a Hamamatsu R3896 tube. The emission spectra were corrected for the instrumental response by calibration with an NBS standard quartz−halogen lamp.

Time-Resolved Emission and Absorption Spectroscopy. Nanosecond flash photolysis transient absorption spectra were measured by irradiating the sample with 6−8 ns (fwhm) of a Continuum Surelight Nd:YAG laser (10 Hz repetition rate) and using as probe light a pulsed Xe lamp perpendicular to the laser beam. The desired excitation wavelength was obtained by frequency doubling (532 nm) or tripling (355 nm). The 150 W Xe lamp was equipped with an Photophysics Model 408 power supply and Photophysics Model 410 pulsing unit (giving pulses of 0.5 ms). A shutter, Oriel Model 71445, placed between the lamp and the sample was opened for 100 ms to prevent PMT fatigue and photodecomposition. Suitable pre- and post-cutoff and band-pass filters were used to prevent photodecompostion and scatter light from the laser. The orientation of the films was 45° with respect to the laser and probe light, set up in the way that the scattered light was reflected to the probe light. In this way we were also able to measure in the early time domain ($t < 50$ ns) without measuring artifacts due to scattered light. The sampling rate was kept relatively long (intervals of 1 or 5 s) to allow complete recovery of the photoinduced transients. The light was collected in a LDC Analytical monochromator and detected by a R928 PTM (Hamamatsu). The laser oscillator, Q-switch, lamp, shutter, and trigger were externally controlled with a digital logic circuit that allowed for synchronous timing. The absorption transients were plotted as $\Delta A = \log(I_o/I_t)$ vs time, where I_o was the monitoring light intensity prior the laser pulse and I_t was the observed signal at delay time t. The same setup as described above was employed for the time-resolved emission experiments, with the exception that the probe lamp was not used. The above-described setup is the one used in the laboratory at the University of Ferrara. Some of the measurements were also performed, with a similar apparatus, in the laboratory at Johns Hopkins University, Baltimore. Perfect agreement was always found between measurements made in the two laboratories.

Results

In the rest of the paper, the mononuclear model and dyads will be indicated as $Ru^{II}(dcb)_2(dmb)$, $Rh^{III}(dcb)_2$-(BL)-$Ru^{II}(bpy)_2$, and $Rh^{III}(dcb)_2$-(BL)-$Ru^{II}(dmp)_2$ (Figure 2), while the same species adsorbed on titanium dioxide films will be indicated as TiO_2-$Ru^{II}(dcb)_2(dmb)$, TiO_2-$Rh^{III}(dcb)_2$-(BL)-$Ru^{II}(bpy)_2$, and TiO_2-$Rh^{III}(dcb)_2$-(BL)-$Ru^{II}(dmp)_2$, respectively.

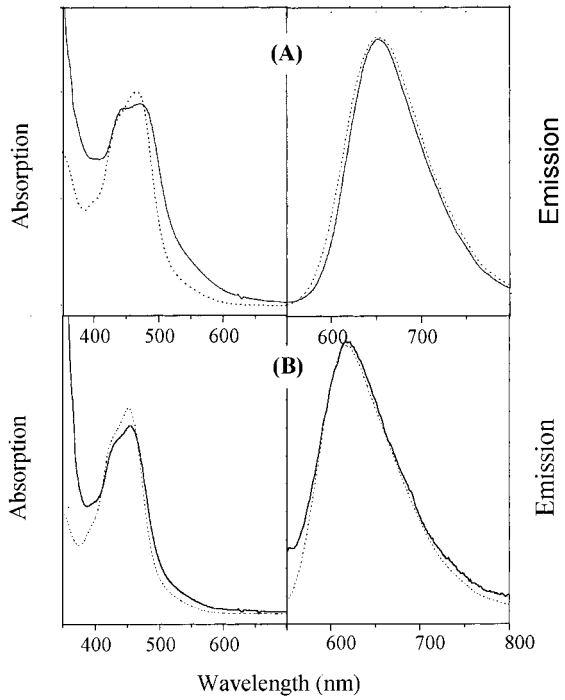

Figure 3. Comparison between spectral profiles in solution and on TiO_2. Absorption (left) and emission (right) profiles of (A) $Ru^{II}(dcb)_2$-(dmb) (···) and TiO_2-$Ru^{II}(dcb)_2$(dmb) (—) and (B) $Rh^{III}(dcb)_2$-(BL)-$Ru^{II}(bpy)_2$ (···) and TiO_2-$Rh^{III}(dcb)_2$-(BL)-$Ru^{II}(bpy)_2$ (—). Solvent: MeOH. All spectra (intensity in arbitrary units) are normalized for purposes of comparison. For details about actual relative intensities, see the text.

UV−Vis Absorption Spectra. The absorption spectra of the $Ru^{II}(dcb)_2(dmb)$ mononuclear model and that of the $Rh^{III}(dcb)_2$-(BL)-$Ru^{II}(bpy)_2$ dyad are depicted in Figure 3, together with those of the same species anchored on TiO_2. The spectrum of $Ru^{II}(dcb)_2(dmb)$ is somewhat red-shifted relative to the those of $Rh^{III}(dcb)_2$-(BL)-$Ru^{II}(bpy)_2$ and $Rh^{III}(dcb)_2$-(BL)-$Ru^{II}(dmp)_2$, as expected on the basis of the better electron acceptor character of dcb relative to bpy or dmp.[57] The spectrum of TiO_2-Ru^{II}-$(dcb)_2(dmb)$, aside from some absorption by TiO_2 at $\lambda \leq 400$ nm, is very similar to that of the model complex in solution, with some broadening, splitting, and red shift of the metal-to-ligand charge transfer (MLCT) band system, as expected on the basis of interaction of the two dcb ligands with the surface. The visible absorption spectrum of the $Rh^{III}(dcb)_2$-(BL)-$Ru^{II}(bpy)_2$ dyad (as well as that of $Rh^{III}(dcb)_2$-(BL)-Ru^{II}-$(dmp)_2$, not shown in Figure 3) is due to MLCT transitions of the Ru(II) component, as the (ligand-centered) transitions of the Rh(III) component are expected in the region $\lambda \leq 350$ nm.[51] Aside from the usual absorption by TiO_2 at $\lambda \leq 400$ nm, the spectrum of TiO_2-$Rh^{III}(dcb)_2$-(BL)-$Ru^{II}(bpy)_2$ is practically identical with that of the corresponding dyad in solution, without any appreciable splitting or red shift. This is consistent with the fact that attachment to the surface takes place via the nonchromophoric Rh(III) component. The experiments described in the following sections involve excitation with visible light, implying, for all systems, selective excitation of the Ru(II) chromophore.

Photoelectrochemical Properties. Figure 4 displays plots of the incident-photon-to-current-efficiency, IPCE(%), vs excitation wavelength for the model complex and dyads on TiO_2 (see

(57) Thus, $Ru^{II}(dcb)_2(dmb)$ cannot strictly be considered a perfect model for the Ru(II) chromophore in the dyads. It is, however, the best model available that also includes anchoring capabilities on TiO_2.

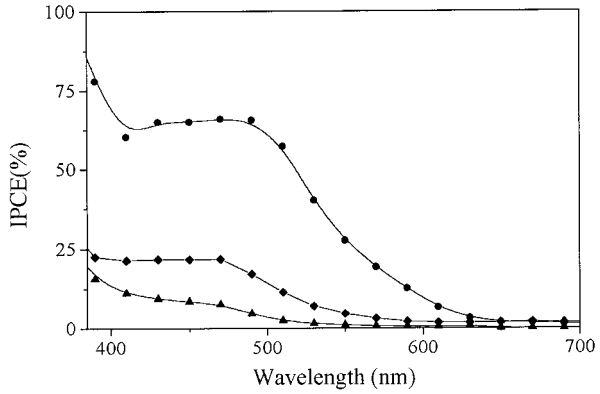

Figure 4. Incident-photon-to-current-efficiency vs the excitation wavelength, IPCE(%), for (●) $Ru^{II}(dcb)_2(dmb)$, (▲) $Rh^{III}(dcb)_2$-(BL)-$Ru^{II}(bpy)_2$, and (◆) $Rh^{III}(dcb)_2$-(BL)-$Ru^{II}(dmp)_2$.

Experimental Section for experimental arrangement and conditions). This quantity is defined as[48]

$$\text{IPCE}(\%) = \frac{1.24 \times 10^3\ (\text{eV·nm}) \times \text{photocurrent density}\ (\mu\text{A·cm}^{-2})}{\text{wavelength (nm)} \times \text{photon flux}\ (\text{W·m}^{-2})} \quad \text{(I)}$$

Figure 4 demonstrates that for TiO_2-$Ru^{II}(dcb)_2(dmb)$, TiO_2-$Rh^{III}(dcb)_2$-(BL)-$Ru^{II}(bpy)_2$, and TiO_2-$Rh^{III}(dcb)_2$-(BL)-$Ru^{II}(dmp)_2$, the photocurrent action spectra closely resemble the absorption spectra of the dye molecules attached to the TiO_2. Absorption maxima and absorbance values for the samples examined were as follows: TiO_2-$Ru^{II}(dcb)_2(dmb)$, $\lambda_{max} = 466$ nm, $A = 1.14$; TiO_2-$Rh^{III}(dcb)_2$-(BL)-$Ru^{II}(bpy)_2$, $\lambda_{max} = 445$ nm, $A = 0.44$; and TiO_2-$Rh^{III}(dcb)_2$-(BL)-$Ru^{II}(dmp)_2$, $\lambda_{max} = 456$ nm, $A = 0.74$.

Emission Measurements. Figure 3 shows a comparison between normalized emission spectra of $Ru^{II}(dcb)_2(dmb)$, $Rh^{III}(dcb)_2$-(BL)-$Ru^{II}(bpy)_2$, TiO_2-$Ru^{II}(dcb)_2(dmb)$, and TiO_2-$Rh^{III}(dcb)_2$-(BL)-$Ru^{II}(bpy)_2$ in MeOH. The emission spectra of $Ru^{II}(dcb)_2(dmb)$ and $Rh^{III}(dcb)_2$-(BL)-$Ru^{II}(bpy)_2$ in solution have the typical aspect of Ru(II) polypyridine MLCT emissions, with maxima at 650 and 620 nm, respectively (615 nm for $Rh^{III}(dcb)_2$-(BL)-$Ru^{II}(dmp)_2$ not shown in Figure 3). Figure 3 shows that band shapes and emission maxima remain practically unaltered, for all the species, upon binding to TiO_2. This is not true, however, for the emission intensities, where model and dyads behave quite differently. Within the uncertainty related to the comparison between solution and solid samples, the emission intensity of the dyads is appreciably the same in solution and on TiO_2, whereas that of the $Ru^{II}(dcb)_2(dmb)$ model is strongly quenched [$I(\text{sol})/I(TiO_2) =$ ca. 0.1].

Time-resolved decays, measured at the maxima of the emission bands under comparable experimental conditions ($\lambda_{exc} = 532$ nm, MeOH), are shown in Figure 5. The emission of $Ru^{II}(dcb)_2(dmb)$ follows a single-exponential decay with a lifetime of 700 ns (MeOH). As expected,[51] the emission of the dyads in solution is strongly quenched relative to the mononuclear model. The emission decay kinetics for $Rh^{III}(dcb)_2$-(BL)-$Ru^{II}(bpy)_2$ and $Rh^{III}(dcb)_2$-(BL)-$Ru^{II}(dmp)_2$ are biexponential (a feature common to analogous dyads, probably related to conformational freedom[51]). Lifetimes and amplitudes in MeOH are as follows: $Rh^{III}(dcb)_2$-(BL)-$Ru^{II}(bpy)_2$, 25 (65%) and 210 ns (35%), and $Rh^{III}(dcb)_2$-(BL)-$Ru^{II}(dmp)_2$, 15 ns (68%) and 120 ns (32%).

When anchored on TiO_2, the shape and position of the emission bands remain almost unaltered, both for the model and for the dyads (Figure 3). By contrast, the effects on decay kinetics are strikingly different between model and dyads. The model complex $Ru^{II}(dcb)_2(dmb)$ shows a clear quenching of the MLCT excited state upon binding to TiO_2, as expected for electron injection. The emission decay of TiO_2-$Ru^{II}(dcb)_2(dmb)$ (MeOH) is complex (as is frequently the case for heterogeneous systems of this type[58]) but clearly much faster than that in solution (Figure 5A).[59] By contrast, the emission decays of the dyads bound to TiO_2 are practically the same as those in solution (see Figure 5B,C). In a biexponential analysis of the decays, lifetimes and amplitudes are as follows: TiO_2-$Rh^{III}(dcb)_2$-(BL)-$Ru^{II}(bpy)_2$ (MeOH), 30 (66%) and 185 ns (34%), and TiO_2-$Rh^{III}(dcb)_2$-(BL)-$Ru^{II}(dmp)_2$ (MeOH), 15 (75%) and 120 ns (25%).

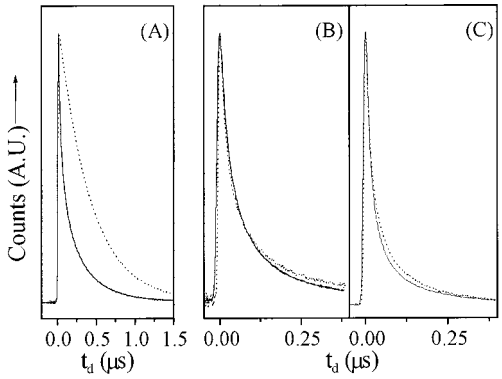

Figure 5. Time-resolved emission decays in MeOH of (A) $Ru^{II}(dcb)_2$-(dmb) (···) and TiO_2-$Ru^{II}(dcb)_2(dmb)$ (—), (B) $Rh^{III}(dcb)_2$-(BL)-$Ru^{II}(bpy)_2$ (···) and TiO_2-$Rh^{III}(dcb)_2$-(BL)-$Ru^{II}(bpy)_2$ (—), and (C) $Rh^{III}(dcb)_2$-(BL)-$Ru^{II}(dmp)_2$ (···) and TiO_2-$Rh^{III}(dcb)_2$-(BL)-$Ru^{II}(dmp)_2$ (—).

When going to MeCN/0.1 M $LiClO_4$ (a solvent system similar to that used in photoelectrochemical experiments), the same general behavior is observed as in MeOH, i.e., strong quenching upon binding to TiO_2 for the mononuclear model but not for the dyads. Lifetimes are generally shorter, however, in this solvent. In particular, for TiO_2-$Ru^{II}(dcb)_2(dmb)$ the emission is completely quenched within the laser pulse. For both $Rh^{III}(dcb)_2$-(BL)-$Ru^{II}(bpy)_2$ and TiO_2-$Rh^{III}(dcb)_2$-(BL)-$Ru^{II}(bpy)_2$ the major decay component has a lifetime of ca. 25 ns, while for both $Rh^{III}(dcb)_2$-(BL)-$Ru^{II}(dmp)_2$ and TiO_2-$Rh^{III}(dcb)_2$-(BL)-$Ru^{II}(dmp)_2$ the decay kinetics could not be resolved with our equipment ($\tau \leq 5$ ns). Time-resolved emission spectra in MeCN/0.1 M $LiClO_4$ are described in the section on transient absorption measurements (where emission is monitored as an apparent bleaching).

Transient Absorption Measurements. These measurements were performed in MeCN/0.1 M $LiClO_4$, a solvent system similar to that used in the photoelectrochemical experiments. The behavior of the model compound $Ru^{II}(dcb)_2(dmb)$ and the dyads in solution was straightforward. The transient absorption

(58) (a) O'Regan, B.; Moser, J. E.; Anderson, M.; Grätzel, M. *J. Phys. Chem.* **1990**, *94*, 8720. (b) Argazzi, R.; Bignozzi, C. A.; Heimer, T. A.; Castellano, F. N.; Meyer G. J. *J. Phys. Chem.* **1994**, *33*, 5741. (c) Yan, S. G.; Hupp, J. T. *J. Phys. Chem.* **1996**, *100*, 6967. (d) Ford, W. E.; Wessels, J. M.; Rodgers, M. A. *J. Phys. Chem. B* **1997**, *101*, 7435.

(59) It should be pointed out that the decays reported in Figure 5 for homogeneous and heterogeneous experiments are normalized to the same "initial" intensity. With complex decay kinetics, this may be somewhat misleading. The quenching of TiO_2-$Ru^{II}(dcb)_2(dmb)$ relative to $Ru^{II}(dcb)_2$-(dmb), though clearly seen as an acceleration of the emission decay, is somewhat underemphasized in Figure 5A. From parallel transient absorption measurements, it can be concluded that in this experiment about 50% of the TiO_2-$Ru^{II}(dcb)_2(dmb)$ excited states have already disappeared within the laser pulse. Thus, what is monitored in Figure 5A is just the long tail portion of a strongly quenched emission.

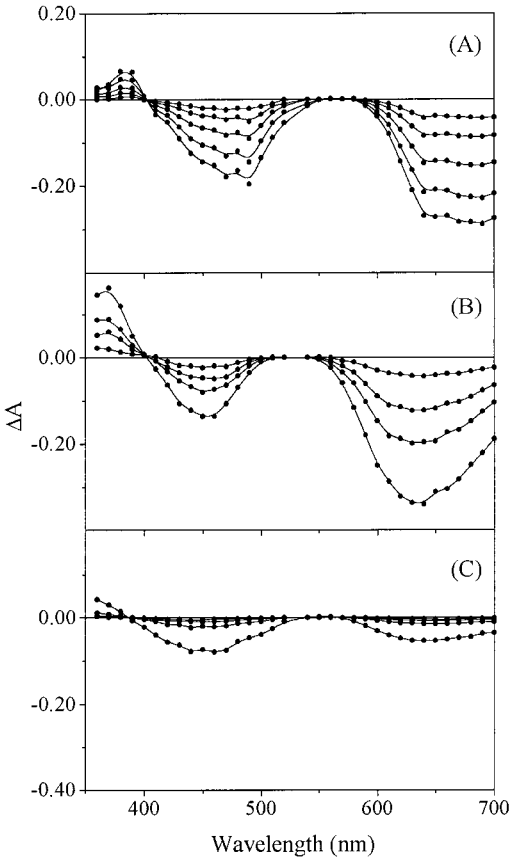

Figure 6. Time-resolved transient absorption spectra in MeCN/0.1 M $LiClO_4$ of (A) $Ru^{II}(dcb)_2(dmb)$ at $\tau_d = 0$, 100, 250, 450, and 700 ns, (B) $Rh^{III}(dcb)_2$-(BL)-$Ru^{II}(bpy)_2$ at $\tau_d = 0$, 20, 40, and 70 ns, and (C) $Rh^{III}(dcb)_2$-(BL)-$Ru^{II}(dmp)_2$ at $\tau_d = 0$, 20, 40, and 70 ns. Optically matched solutions at $\lambda_{exc} = 532$ nm, $P = 10$ mJ/pulse.

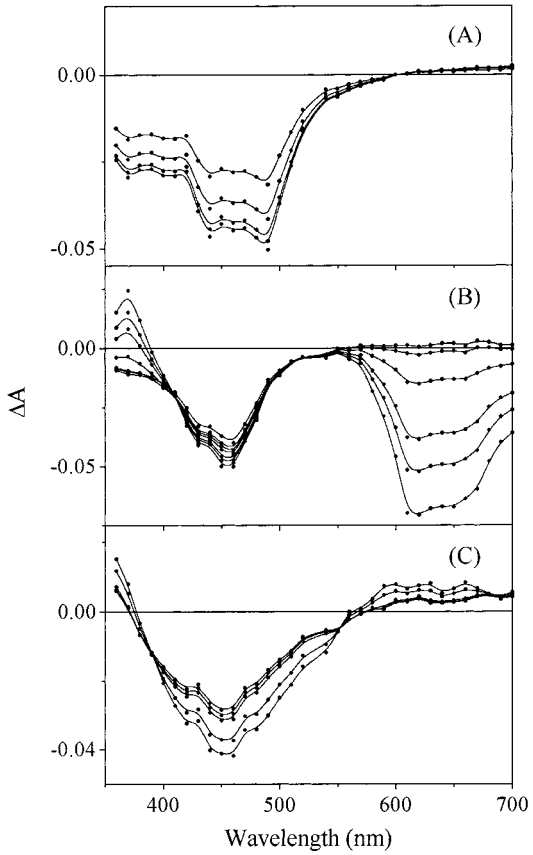

Figure 7. Time-resolved transient absorption spectra in MeCN/0.1 M $LiClO_4$ of (A) TiO_2-$Ru^{II}(dcb)_2(dmb)$ at $\tau_d = 0$, 100, 500, and 2000 ns, (B) TiO_2-$Rh^{III}(dcb)_2$-(BL)-$Ru^{II}(bpy)_2$ at $\tau_d = 0$, 10, 20, 50, 100, 500, and 2000 ns, and (C) TiO_2-$Rh^{III}(dcb)_2$-(BL)-$Ru^{II}(dmp)_2$ at $\tau_d = 0$, 100, 500, 1000, and 2000 ns. $\lambda_{exc} = 532$ nm, $P = 1$ mJ/pulse.

spectra of model and dyads are depicted in Figure 6. They all show a positive absorption at ca. 370 nm and a strong bleaching centered at ca. 450 nm. This behavior, arising from the appearance of transitions of the polypyridine radical-anion and the disappearance of ground-state MLCT transitions, is typical of the formation of the triplet MLCT excited state of Ru(II) polypyridine chromophores.[60] The apparent bleachings observed at $\lambda > 550$ nm, where all the samples have negligible absorption before the pulse, is actually due to light emission from the samples.[61] In all cases, the decay kinetics of the transient absorbance changes closely match that of the emission. Lifetimes obtained from the transient absorption measurements in MeCN/0.1 M $LiClO_4$ solution are as follows: $Ru^{II}(dcb)_2(dmb)$, 310 ns; $Rh^{III}(dcb)_2$-(BL)-$Ru^{II}(bpy)_2$, 30 ns (complex decay, main component) and $Rh^{III}(dcb)_2$-(BL)-$Ru^{II}(dmp)_2$, <10 ns (complex decay, substantial transient already lost at $t = 0$).

The transient absorption spectra of the adsorbed species TiO_2-$Ru^{II}(dcb)_2(dmb)$, TiO_2-$Rh^{III}(dcb)_2$-(BL)-$Ru^{II}(bpy)_2$, and TiO_2-$Rh^{III}(dcb)_2$-(BL)-$Ru^{II}(dmp)_2$, measured in MeCN/0.1 M $LiClO_4$, are depicted in Figure 7. The transient spectrum of TiO_2-$Ru^{II}(dcb)_2(dmb)$ (Figure 7A) is clearly different from that of the model in solution (Figure 6A). It is as expected for complete (95%) formation of $TiO_2(e^-)$-$Ru^{III}(dcb)_2(dmb)$: bleaching of the MLCT absorption, lack of polypyridine radical anion absorption at ca. 370 nm, no apparent bleaching at $\lambda > 600$ nm due to emission, and weak absorption at $\lambda > 600$ nm arising from the oxidized Ru(III) species[62] with some possible contribution from the electron injected into TiO_2.[63] The transient spectral changes for TiO_2-$Ru^{II}(dcb)_2(dmb)$ decay with time-resolved profiles independent of wavelength, but with complex kinetics, as usual for this type of heterogeneous systems.[58] Most of the bleaching recovers in a few microseconds (with an approximate lifetime of ca. 7 μs[64]), but the remaining portion requires milliseconds to revert to the initial baseline (Figure 8A).

The transient absorption spectra of TiO_2-$Rh^{III}(dcb)_2$-(BL)-$Ru^{II}(bpy)_2$ (Figure 7B) also differ from those of the dyad in

(60) Braterman, P. S.; Harriman, A.; Heath G. A.; Yellowless L. *J. Chem. Soc., Dalton Trans.* **1983**, 1801. Kalyanasundaram, K. *Photochemistry of Polypyridine and Porphyrin Complexes*; Academic: New York, 1992.

(61) Some caveats are appropriate when emission is monitored as an apparent bleaching in transient absorption spectroscopy. (i) It should be pointed out that, while true absorbance changes are independent of instrumental settings such as monochromator slits and photomultiplier gain, the magnitude of any emission-related apparent bleaching strongly depends on such parameters. Thus, the ratio between the magnitudes of true and apparent bleachings in transient spectra such as those of Figure 6 is *not* a molecular property. (ii) The emission profiles, as obtained from such apparent bleachings, may not exactly coincide with those obtained from classical emission measurements. In fact, the protocol used in the transient absorption measurements (at any wavelength, I_0 is set to a constant value by adjusting the photomultiplier gain) results in a wavelength-dependent amplification. (iii) The decay kinetics of the apparent bleaching, $\log I_0 - \log I(t)$, is not expected to parallel exactly that of a true emission signal, $I(t)$, except for the "optically diluted" limit (i.e., apparent bleachings with $\Delta A \leq 0.1$).

(62) McCaffery, A. J.; Mason, S. F.; Norman, B. J. *J. Chem. Soc. A* **1969**, 1428.

(63) Rothenberger, G.; Fitzmaurice, D.; Grätzel, M. *J. Phys. Chem.* **1992**, *96*, 5983.

(64) The behavior was not strictly exponential in the time interval of 0−2 μs. Although other kinetic models (e.g., Kohlrausch−Williams−Watts, second order) could be used as well, a good fit was obtained with a biexponential function. At 1 mJ/pulse laser power, the fit gave the following lifetimes and relative amplitudes: $\tau_1 = 0.38$ μs (16%), $\tau_2 = 6.8$ μs (84%).

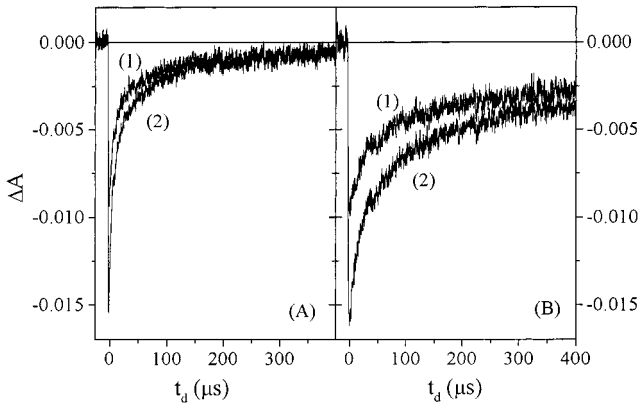

Figure 8. The microsecond decay kinetics in MeCN/0.1 M $LiClO_4$ of (A) TiO_2-$Ru^{II}(dcb)_2(dmb)$ and (B) TiO_2-$Rh^{III}(dcb)_2$-(BL)-$Ru^{II}(bpy)_2$. Measured at 450 nm, with 532-nm excitation, $P = 1$ mJ/pulse (lower trace), and 0.3 mJ/pulse (upper trace).

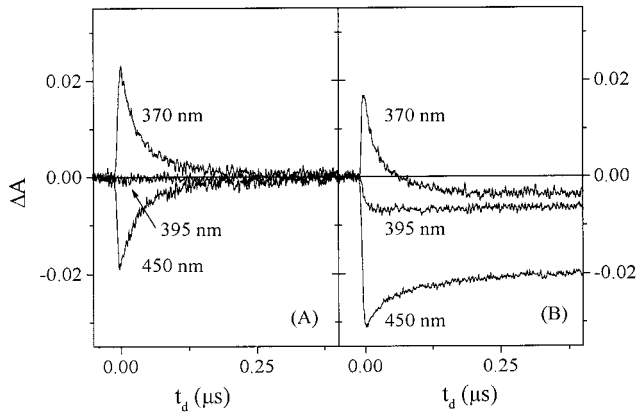

Figure 9. Kinetic traces at selected wavelengths of (A) $Rh^{III}(dcb)_2$-(BL)-$Ru^{II}(bpy)_2$ (see spectral changes of Figure 6B) and (B) TiO_2-$Rh^{III}(dcb)_2$-(BL)-$Ru^{II}(bpy)_2$ (see spectral changes of Figure 7B).

solution, but less markedly than in the mononuclear model case. The transient absorption difference spectrum of TiO_2-$Rh^{III}(dcb)_2$-(BL)-$Ru^{II}(bpy)_2$ observed at $\tau_d = 0$ ns shows positive absorption centered at 370 nm and bleaching centered at 450 nm. The apparent bleaching observed at $\lambda > 550$ nm is, as in the solution experiments, due to light emission from the sample.[61] These initial spectral changes, coupled with the observation of emission, suggest initial formation of the MLCT excited state of the Ru(II) unit. That the situation is not as simple as in the free dyad is demonstrated, however, by the different ratios of absorption to bleaching (Figure 9) and by the definite absorbance decrease observed at 395 nm (where the ground and MLCT excited state have an isosbestic point, see Figure 6B). In the early time regime (0−100 ns) the spectral changes decay with a lifetime of ca. 25 ns (Figure 9) to an intermediate product spectrum with bleaching at both 370 and 450 nm. With the same lifetime, the observed emission disappears (Figure 7B). On a much longer time scale, the residual spectral changes decay with complex kinetics to the original baseline (Figure 8B).

Excitation of TiO_2-$Rh^{III}(dcb)_2$-(BL)-$Ru^{II}(dmp)_2$ in MeCN/0.1 M $LiClO_4$ results in a transient absorption spectrum as is shown in Figure 7C. The main differences with respect to TiO_2-$Rh^{III}(dcb)_2$-(BL)-$Ru^{II}(bpy)_2$ are as follows: (i) at $t = 0$ no emission is observed at $\lambda > 550$ nm and (ii) very few spectral changes take place in the early time regime (0−100 ns). This indicates that with this dyad practically no MLCT excited state is present after the laser pulse. On a much longer time scale, the transient spectrum reverts to the initial baseline, with a complex kinetics, analogous to that of the other system.

Finally, it should be pointed out that, in all cases, the complex kinetics for the recovery of the transient spectral changes in the long time domain (microsecond to millisecond) was strongly dependent on the laser power used. This is shown in Figure 8 for TiO_2-$Ru^{II}(dcb)_2(dmb)$ and TiO_2-$Rh^{III}(dcb)_2$-(BL)-$Ru^{II}(bpy)_2$, by comparing results obtained at 0.3 to 1.0 mJ·cm^{-2}. The general trend is that the weight of the microsecond component, relative to the ms one, decreases with decreasing laser power.

Discussion

Dyads in Solution. The first step in this work has been to verify the behavior of the $Rh^{III}(dcb)_2$-(BL)-$Ru^{II}(dmp)_2$ and $Rh^{III}(dcb)_2$-(BL)-$Ru^{II}(bpy)_2$ dyads in solution. A thorough kinetic characterization was previously made for the related dyad $Rh^{III}(dmb)_2$-BL-$Ru^{II}(dmp)_2$.[51] Although the change in terminal ligands may bring about minor changes in energetics, and thus in rate constants, the general behavior expected upon visible excitation of the Ru(II)-based chromophore is the following: photoinduced electron transfer to the Rh(III) unit (eq 1), with

$$\text{Rh(III)-*Ru(II)} \rightarrow \text{Rh(II)-Ru(III)} \quad (1)$$

substantial quenching of the Ru(II) metal-to-ligand charge transfer (MLCT) state, and fast back electron transfer (eq 2),

$$\text{Rh(II)-Ru(III)} \rightarrow \text{Rh(III)- Ru(II)} \quad (2)$$

preventing the observation of Rh(II)-Ru(III) intermediate in transient experiments. Indeed, in both dyads the MLCT state of the Ru(II) chromophore is strongly quenched. Although the emission decays are appreciably nonexponential (probably because of conformational freedom at the BL bridge[51]), for both $Rh^{III}(dcb)_2$-(BL)-$Ru^{II}(bpy)_2$ and $Rh^{III}(dcb)_2$-(BL)-$Ru^{II}(dmp)_2$ the major component (ca. 70%) has lifetimes shorter than 30 ns (Figures 5 and 6B,C). This is to be compared with lifetimes in the microsecond range for mononuclear Ru(II) model systems (e.g., $Ru^{II}(dcb)_2(dmb)$ in Figure 5A;[57] see also, e.g.,[51] $Ru^{II}(dmp)_2$-(BL), 1.8 μs). When the decay of the MLCT excited state is monitored by time-resolved absorption spectroscopy (Figure 6), the clean spectral changes correspond to conversion of the MLCT state to ground state processes, with decay times comparable to those obtained from emission, as expected assuming a sequence of forward (eq 1, rate determining) and back (eq 2, fast) electron transfer. The increase in excited-state decay rate observed in going from the bpy-containing system to the dmp-based one (Figures 5 and 6, B vs C) is consistent with the expected decrease in Ru(III)/(II) potential and the corresponding increase in driving force for photoinduced electron transfer.[65,66] The lifetimes of the model and dyads are somewhat dependent on the solvent used (MeOH vs MeCN),[67] but the relative ordering $Ru^{II}(dcb)_2(dmb) \gg Rh^{III}(dcb)_2$-(BL)-$Ru^{II}(bpy)_2 > Rh^{III}(dcb)_2$-(BL)-$Ru^{II}(dmp)_2$ remains the same (Figures 5 and 6). In conclusion, the two dyads behave in solution as expected on the basis of molecular design. Of particular interest is the modulation of the photoinduced electron transfer kinetics achieved by applying relatively minor changes (bpy vs dmp) at the Ru(II) center.

(65) The difference in Ru(III)/Ru(II) potential can be estimated as ca. 100 mV, by extrapolation from the electrochemistry of the tris-homoleptic bpy and dmp Ru(II) complexes.[66] The difference in excited-state redox potential is probably somewhat smaller, because of partial compensation in the energy of the MLCT state.

(66) Lin, C.-T.; Böttcher, W.; Chou, M.; Creutz, C.; Sutin, N. *J. Am. Chem. Soc*. **1976**, *98*, 6536.

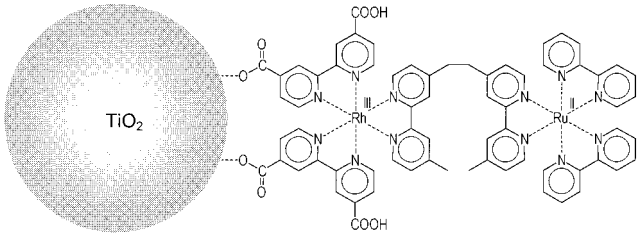

Figure 10. Schematic picture of TiO_2-$Rh^{III}(dcb)_2$-(BL)-$Ru^{II}(bpy)_2$ on TiO_2 as a heterotriad system.

Behavior on Titanium Dioxide. The $Rh^{III}(dcb)_2$-(BL)-$Ru^{II}(bpy)_2$ and $Rh^{III}(dcb)_2$-(BL)-$Ru^{II}(dmp)_2$ dyads adsorb to nanoporous titanium dioxide films under standard experimental conditions. We surmise that the main interaction responsible for chemisorption is the coordination of carboxylate groups to Ti(IV) centers on the surface. Indeed, complexes lacking such groups, such as, e.g., $Rh^{III}(dmb)_2$-(BL)-$Ru^{II}(dmp)_2$, do not adsorb appreciably under comparable conditions. This implies that surface attachment of the dyads occurs at the Rh(III) unit. The Ru(II) unit, also because of its positive charge, is likely to be, in the average conformation of the adsorbed dyads, at a greater distance from the surface of the TiO_2 nanoparticles. Thus, these adsorbed species can be structurally considered as TiO_2-Rh(III)-Ru(II) heterotriads, as schematically shown in Figure 10.[68] With respect to a mononuclear sensitizer such as, e.g., $Ru^{II}(dcb)_2$-(dmb), the dyads seem to adsorb to a smaller degree (typically ca. 50%). This is probably due to the unfavorable overall charge of the dyads as compared to the mononuclear species (neutral, under similar assumptions). Other reasons, e.g., differences in surface coverage due to the larger molar volume and nonideal orientation of the dyads, cannot be ruled out, however.

The fact that both dyads inject electrons into TiO_2 following light absorption by the Ru(II)-based chromophore is clearly demonstrated by photocurrent action spectra (Figure 4). The smaller photocurrent efficiency of the dyads, as compared with mononuclear $Ru^{II}(dcb)_2(dmb)$, is only partly due to smaller light absorption. After correction for this effect, the absorbed photon-to-electron conversion efficiencies are still 19% for $Rh^{III}(dcb)_2$-(BL)-$Ru^{II}(bpy)_2$ and 31% for $Rh^{III}(dcb)_2$-(BL)-$Ru^{II}(dmp)_2$, as compared to 85% for $Ru^{II}(dcb)_2(dmb)$. The photocurrent efficiency in a regenerative solar cell is a complex function of many factors.[18] One such factor is the electron injection efficiency, and a reduction in this efficiency may be, at least partially, responsible for the low photocurrents obtained with the dyads. Reasons for this behavior will be discussed below.

Mechanism of Electron Injection. The mechanism of electron injection from the dyads deserves a detailed discussion. In an idealized geometry such as that of Figure 10, the large distance of the Ru(II) unit from the surface suggests *stepwise injection* (i.e., "heterotriad" behavior, eqs 3 and 4) as a plausible mechanism. The possibility of *direct injection* from the excited chromophore (eq 5), however, cannot be discarded on an a priori basis. With simple mononuclear sensitizers, subpicosecond

$$TiO_2\text{-Rh(III)-*Ru(II)} \rightarrow TiO_2\text{-Rh(II)-Ru(III)} \quad (3)$$

$$TiO_2\text{-Rh(II)-Ru(III)} \rightarrow TiO_2(e^-)\text{-Rh(III)- Ru(III)} \quad (4)$$

$$TiO_2\text{-Rh(III)-*Ru(II)} \rightarrow TiO_2(e^-)\text{-Rh(III)- Ru(III)} \quad (5)$$

$$TiO_2\text{-Rh(II)-Ru(III)} \rightarrow TiO_2\text{-Rh(III)-Ru(II)} \quad (6)$$

electron injection has been observed following excitation.[69] Such ultrafast rates are probably related to fact that the grafting groups provide strong electronic coupling between the semiconductor and the π^* orbital where the excited electron is localized upon excitation. Less detailed information is available on injection rates from sensitizer units not directly grafted onto the surface. These processes are presumably slower, but could nevertheless be efficient for long-lived excited states. For instance, in the case of $Re^{I}(dcb)(CO)_3$-(CN)-$Ru^{II}(bpy)_2(CN)$,[70] anchored to the TiO_2 surface via the Re-based unit, efficient electron injection has been reported to occur from the "remote"[71] Ru-based chromophore.

Experimentally, the discrimination between direct and stepwise injection is not trivial. In principle, a comparison between the behavior of the heterogeneous system and that of the dyad in solution could be used for this purpose. If electron injection occurs stepwise (eqs 3 and 4), the MLCT excited state of the dyad on TiO_2 should have comparable properties (emission yield, lifetime) as in solution. In the case of direct injection (eq 5), the MLCT state of the dyad on TiO_2 is expected to be strongly quenched with respect to solution. When the comparison between heterogeneous phase and solution is based on emission decays (Figure 5) the result is that $\tau[TiO_2\text{-Rh(III)-*Ru(II)}] \approx \tau[\text{Rh(III)-*Ru(II)}]$. This is true for both dyads, with the shorter lifetime of the $Rh^{III}(dcb)_2$-(BL)-$Ru^{II}(dmp)_2$ system as compared to $Rh^{III}(dcb)_2$-(BL)-$Ru^{II}(bpy)_2$ being maintained in the heterogeneous phase. This seems to bring strong support to a stepwise mechanistic hypothesis (eqs 3 and 4).

When transient absorption measurements (Figures 6 and 7) are used in this comparison, however, a more complex situation appears. Let us use $Rh^{III}(dcb)_2$-(BL)-$Ru^{II}(bpy)_2$ (Figures 6B and 7B) for a detailed analysis. As discussed above, the transient spectral changes of the dyad in solution (positive absorption at $\lambda = 370$ nm, isosbestic point at $\lambda = 395$ nm, and bleaching at $\lambda = 450$ nm, Figure 6B) represent prompt formation of the Ru-based MLCT state, followed by decay to the ground state via a sequence of forward (eq 1, rate determining) and back (eq 2, fast) electron-transfer processes. On TiO_2 (Figure 7B), substantially different spectral changes are observed: the initial spectrum resembles but is not identical with, that of the MLCT state. In particular, as shown in detail in Figure 9, the ratio of positive absorption to bleaching is smaller, and at 395 nm, where no spectral change should be expected upon conversion of ground state to MLCT, a definite bleaching is observed. These spectral changes can be easily understood if it is assumed that,

(67) The solvent can affect excited-state decay kinetics in several ways. Peculiar to dcb-based systems is the possibility that the solvent affects the degree of protonation of the carboxylic groups. In the case of the mononuclear model, this is expected to affect the MLCT excited-state energy, and thus the energy gap for radiationless deactivation. In the dyads, this is expected to affect Rh(III)/(II) redox potential, and thus the driving force of the intramolecular electron transfer step. In aqueous media, where the protonation of the carboxylic groups can be precisely controlled, a gradual acceleration in decay rate with increasing degree of protonation has been demonstrated for the dyads (M. T. Indelli, unpublished results).

(68) While the carboxylate groups grafted to the surface are certainly deprotonated, the actual number of groups grafted and the overall state of protonation are not known. The arrangement of Figure 10 has simply been chosen for graphical purposes.

(69) (a) Eichberger, R.; Willig, F. *Chem. Phys.* **1990**, *141*, 159. (b) Tachibana, Y.; Moser, J. E.; Grätzel, M.; Klug, D. R.; Durrant, J. R. *J. Phys. Chem.* **1996**, *100*, 20056. (c) Rehm, J. M.; McLendon, G. L.; Nagasawa, Y.; Yoshihara, K.; Moser, J.; Grätzel, M. *J. Phys. Chem.* **1966**, *100*, 9777.

(70) Argazzi, R.; Bignozzi, C. A.; Heimer, T. A.; Meyer, G. J. *Inorg. Chem.* **1996**, *36*, 2.

(71) It should be noticed, however, that in this case (i) the short cyanide bridge provides very strong metal−metal electronic coupling and (ii) the cis geometry at the Re center between the anchoring dcb and the bridging cyanide ligand brings the Ru-based chormophore very close to the surface.[70]

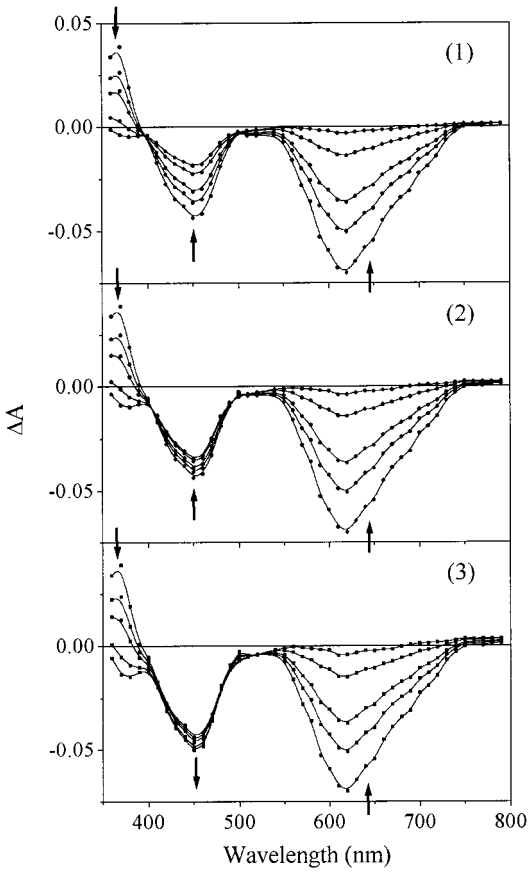

Figure 11. Simulated transient absorption spectra of the TiO_2-Rh^{III}-$(dcb)_2$-(BL)-$Ru^{II}(bpy)_2$ heterotriad after pulsed 532 nm excitation. Delay times in nanoseconds: 0, 10, 20, 50, and 100. Arrows indicate the direction of the spectral changes. The initial spectrum is always calculated assuming 35% prompt injection and 65% Ru(II) MLCT excited-state formation (see text). Panel 1 simulates the spectral changes to be expected if all the MLCT excited states revert to the ground state without injection of electrons into TiO_2 ($F = 0$ in eq 7). Panel 2 simulates the case where half of the MLCT excited states inject electrons into TiO_2 and half go to the ground-state m ($F = 0.5$ in eq 7). Panel 3 simulates the case where all the MLCT excited states inject electrons into TiO_2 ($F = 1$ in eq 7). Details of the simulation are given in the text.

in addition to *Ru(II) MLCT states, oxidized Ru(III) centers are already formed within the laser pulse, i.e., that some direct injection (eq 5) is also taking place in the system. It should be noted that, despite the occurrence of such fast direct injection, the transient decay remains relatively slow, with the same kinetics (τ, ca. 30 ns) for TiO_2-$Rh^{III}(dcb)_2$-(BL)-$Ru^{II}(bpy)_2$ (Figure 9B) as for $Rh^{III}(dcb)_2$-(BL)-$Ru^{II}(bpy)_2$ in solution (Figure 9A), as required by the stepwise mechanism. This implies that the two processes, direct injection and the observable excited-state decay, are kinetically decoupled processes that must involve structurally different heterotriads. Likely situations that may favor direct injection are the following: (i) nonideal orientation of the dyad at the surface and (ii) accidental contacts in small-size cavities. Using the appropriate Ru(II), *Ru(II), and Ru(III) molar absorptivities,[51] the proportion of dyads undergoing direct injection is estimated as ca. 35%.

The rest (ca. 65%) of the excited TiO_2-$Rh^{III}(dcb)_2$-(BL)-$Ru^{II}(bpy)_2$ systems decay, as do the dyads in solution, via intramolecular electron transfer (eq 3). The time constant of this process, as obtained from the transient spectral changes and from the MLCT emission, is 30 ns. Given the long intrinsic lifetime of the MLCT excited state (ca. 1 μs), the efficiency of

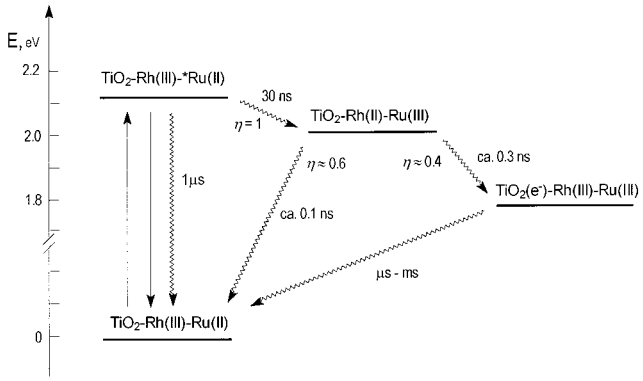

Figure 12. Energy level diagram and photophysical processes for the TiO_2-$Rh^{III}(dcb)_2$-(BL)-$Ru^{II}(bpy)_2$ heterotriad.

photoinduced electron transfer is unitary. As for all triad systems, the fate of the primary electron-transfer product depends on the competition between further charge separation (in this case, charge injection, eq 4) and primary charge recombination (eq 6). From the behavior of related dyads in solution[51] primary charge recombination is known to occur in ca. 100 ps, and thus any competitive charge injection is also expected to occur in the subnanosecond time scale. Therefore, the transient spectral changes in the 0−100 ns interval (Figure 9B) effectively correspond to conversion of the MLCT excited state to a mixture of charge-separated product and ground state, as indicated in eq 7 , where F is the efficiency of charge

$$TiO_2\text{-Rh(III)-*Ru(II)} \rightarrow F TiO_2(e^-)\text{-Rh(III)-Ru(III)} + (1 - F)TiO_2\text{-Rh(III)-Ru(II)} \quad (7)$$

separation (stepwise charge injection) $k_4/(k_4 + k_6)$.[72] Using the appropriate molar absorptivity values,[51] F can be calculated as ca. 0.4 from the spectral changes of Figure 9B. The error on this number is certainly large ($\pm$0.1), but the transient spectral changes are sufficiently diagnostic to demonstrate the occurrence of substantial charge injection after photoinduced electron transfer. This is convincingly illustrated by Figure 11, showing simulated spectral changes[73] for F values of 1 (Figure 11.1), 0.5 (Figure 11.2), and 0 (Figure 11.3). Thus, TiO_2-$Rh^{III}(dcb)_2$-(BL)-$Ru^{II}(bpy)_2$ indeed behaves as a heterotriad system like the one depicted in Figure 1a. The photophysical behavior is summarized in the energy level diagram[74] of Figure 12.

When the behavior of the TiO_2- $Rh^{III}(dcb)_2$-(BL)-$Ru^{II}(dmp)_2$ heterotriad is considered (Figure 7C), the main difference with the previous case is consistent with the behavior of the dyads

(72) This model assumes that no recombination between injected electrons and Ru(III) centers takes place during this period. Considering this assumption, the F value estimated from the transient spectral changes should be taken as a lower limit for the efficiency of stepwise injection.

(73) The spectra were simulated with the constraints that the Ru unit exclusively absorbs light in the visible region and that the spectra of ground, excited, and oxidized states of the Ru(II) polypyridine chromophore are the same as those reported for ruthenium trisbipyridine in acetonitrile (Yoshimura, A.; Hoffman, M. Z.; Sun, H. *J. Photochem. Photobiol. A: Chem.* **1993**, *70*, 29). The emission spectra at longer wavelengths was simulated from the emission spectrum in Figure 3B, with a 25 ns lifetime. The rates of electron injection into TiO_2 (eqs 4 and 5) and of intramolecular back electron transfer (eq 6) were set to be much faster then the instrument response for the measured data. Note that on the 100 ns time scale these data was simulated over, interfacial charge recombination (eq 9) does not alter the simulated spectra, consistent with experimental observations of Figure 9.

(74) The approximate energies in Figure 12 are estimated on the basis of (i) standard values for MLCT excited-state redox potentials,[65] (ii) a measured value of −0.81 V for the Rh(III)/(II) couple in the dyads, and (iii) an assumed redox potential for the conduction band of TiO_2, under our experimental conditions, of −0.50 V vs SCE.

in solution (vide supra). As expected on the basis of the solution experiments, photoinduced electron transfer (eq 3) is now much faster than in the previous dyad, actually too fast to be time-resolved: at $t = 0$ no well-defined maximum at 370 nm is present, no MLCT emission is observed at at $\lambda > 550$ nm, and very few spectral changes are noticed in the 0−100 ns time scale. Thus, in this case, both photoinduced electron transfer and charge separation take place within the laser pulse. The mechanism is probably similar to that depicted in Figure 12, although with a much faster (<5 ns) primary electron-transfer step, and with unknown efficiencies for charge separation and primary recombination.

Charge Recombination. In supramolecular photochemistry, the aim pursued in going from dyads to triads, etc., is to increase distance, and thus the lifetime, of charge separation. From this standpoint, it is interesting to compare the rate of charge recombination in the heterotriad systems (eq 9) with that of appropriate model heterodyads (eq 8). In general, heterogeneous

$$TiO_2(e^-)\text{-}Ru(III) \rightarrow TiO_2\text{-}Ru(II) \quad (8)$$

$$TiO_2(e^-)\text{-}Rh(III)\text{-}Ru(III) \rightarrow TiO_2\text{-}Rh(III)\text{-}Ru(II) \quad (9)$$

charge recombination processes on TiO_2 are known to exhibit complex kinetic behavior. Various laws and models have been proposed to account for this complex kinetics,[58] and their analysis is presently beyond the scope of this paper.[75] The comparison between the charge recombination in TiO_2-$Ru^{III}(dcb)_2$-(dmb) and TiO_2-$Rh^{III}(dcb)_2$-(BL)-$Ru^{II}(dmp)_2$ is shown in Figure 8. It is seen that, as expected, the kinetics for the recovery of the transient absorption bleach is complex and depends strongly on laser power. Regardless of the recombination mechanism and kinetic law, however, it is quite evident that the change from simple mononuclear sensitizer (heterodyad) to a binuclear sensitizer (heterotriad) brings about a huge increase in lifetime of charge separation: for TiO_2-$Ru^{III}(dcb)_2(dmb)$, most of the charge-separated states recombine within a few microseconds; for TiO_2-$Rh^{III}(dcb)_2$-(BL)-$Ru^{II}(dmp)_2$, the time scale for recombination becomes micro- to milliseconds. Together with the results discussed in the previous section, the observation of a markedly enhanced charge separation lifetime brings strong support to the behavior of these systems as heterotriads.

(75) Kleverlaan, C. J, et al. Manuscript in preparation.

Conclusions

This paper provides an example of how the principles of stepwise charge separation, originally developed in the field of supramolecular photochemistry, can be applied to hetero-supramolecular systems involving nanocrystalline semiconductors. The systems studied were designed as proof-of-principle heterotriads, without any pretension to compete with the sensitizers commonly used in regenerative solar cells. In fact, their photocurrent efficiency is rather low, mainly because of low charge injection yields. Nevertheless, they demonstrate a strategy to slow significantly the recombination between injected electron and oxidized sensitizer. In the solar cell, recombination is inhibited by scavenging the oxidized sensitizer with a relay couple in solution. This is made at the following price: (i) a large part of the converted energy is used as the driving force for the scavenging reaction and (ii) some of the incident light is absorbed by the high concentrations of relay species needed. It is likely that some of these losses could be minimized by using suitable supramolecular sensitizers, with intrinsically slower recombination rates.

Acknowledgment. We thank C. Chiorboli and A. Prodi for their assistance in some transient measurements. This work was carried out with financial support from MURST (Progetto Dispositivi Supramolecolari), CNR (Centro di Fotoreattività e Catalisi, Ferrara), and EC (TMRX-CT96-0079). The Division of Chemical Sciences, Office of Basic Energy Sciences, Office of Energy Research, U.S. Department of Energy is gratefully acknowledged for research support. G.M.H. would like to thank the Link foundation for an Energy Fellowship.

JA992755F